Annals of Botany **114**: 1385–1397, 2014
doi:10.1093/aob/mcu172, available online at www.aob.oxfordjournals.org

ANNALS OF BOTANY
Founded 1887

PART OF A SPECIAL ISSUE ON PLANT CELL WALLS

Structures formed by a cell membrane-associated arabinogalactan-protein on graphite or mica alone and with Yariv phenylglycosides

Li Hong Zhou[1,2,3], Renate A. Weizbauer[1,2,4], Srikanth Singamaneni[2], Feng Xu[3,5], Guy M. Genin[2] and Barbara G. Pickard[1,*]

[1]*Gladys Levis Allen Laboratory of Plant Sensory Physiology, Biology Department, Washington University in St. Louis, St. Louis, MO, USA,* [2]*Department of Mechanical Engineering & Materials Science, Washington University in St. Louis, St. Louis, MO, USA,* [3]*Biomedical Engineering & Biomechanics Center, Xi'an Jiaotong University, Xi'an, China,* [4]*Carnegie Institution, Department of Plant Biology, Stanford, CA, USA and* [5]*School of Life Science & Technology, Xi'an Jiaotong University, Xi'an, China*
** For correspondence. E-mail pickard@wustl.edu*

Received: 26 March 2014 Returned for revision: 10 June 2014 Accepted: 3 July 2014 Published electronically: 27 August 2014

• **Background** Certain membrane-associated arabinogalactan-proteins (AGPs) with lysine-rich sub-domains participate in plant growth, development and resistance to stress. To complement fluorescence imaging of such molecules when tagged and introduced transgenically to the cell periphery and to extend the groundwork for assessing molecular structure, some behaviours of surface-spread AGPs were visualized at the nanometre scale in a simplified electrostatic environment.
• **Methods** Enhanced green fluorescent protein (EGFP)-labelled LeAGP1 was isolated from *Arabidopsis thaliana* leaves using antibody-coated magnetic beads, deposited on graphite or mica, and examined with atomic force microscopy (AFM).
• **Key Results** When deposited at low concentration on graphite, LeAGP can form independent clusters and rings a few nanometres in diameter, often defining deep pits; the aperture of the rings depends on plating parameters. On mica, intermediate and high concentrations, respectively, yielded lacy meshes and solid sheets that could dynamically evolve arcs, rings, 'pores' and 'co-pores', and pits. Glucosyl Yariv reagent combined with the AGP to make very large and distinctive rings.
• **Conclusions** Diverse cell-specific nano-patterns of native lysine-rich AGPs are expected at the wall–membrane interface and, while there will not be an identical patterning in different environmental settings, AFM imaging suggests protein tendencies for surficial organization and thus opens new avenues for experimentation. Nanopore formation with Yariv reagents suggests how the reagent might bind with AGP to admit Ca^{2+} to cells and hints at ways in which AGP might be structured at some cell surfaces.

Key words: Plant cell walls, lysine-rich arabinogalactan-protein, LeAGP1, EGFP, atomic force microscopy, glycoprotein cluster, glycoprotein mesh, nanopore, periplasm, Yariv phenylglycoside, *Arabidopsis thaliana*.

INTRODUCTION

The modes of function of arabinogalactan-proteins (AGPs), a group with members participating in the regulation of many major activities of plants, are not well understood. Study has been limited in considerable part by the slow development of technologies for conveniently handling specific members of the sizeable family and observing them at high resolution (Ellis *et al.*, 2010; Tan *et al.*, 2010). One particular kind of AGP, however, invites intensive scrutiny with further microscopy. It is a member of a small group of AGPs that contain a lysine-rich sub-domain (or region). The least ambiguous acronym for one of these glycoproteins is KRR-AGP. The tomato KRR-AGP on which we focus in this report has been particularly well characterized biochemically, and is the only representative of the group in that species (Sun *et al.*, 2004, 2005; Estévez *et al.*, 2006; Tan *et al.*, 2010; Lamport and Várnai, 2013). It has a 173 amino acid peptide containing a 13 amino acid lysine-rich region, and is secreted into the periplast with a glycosylphosphatidylinositol (GPI) link. It has well-described, repetitively positioned, arabinan and arabinogalactan groups; and its three *Arabidopsis thaliana* homologues are also characterized (e.g. Sun *et al.*, 2005; Yang *et al.*, 2007). The ability of the numerous arabinogalactans to bind H^+ or, alternatively, Ca^{2+} at a well-characterized site might be of physiological significance (Lamport and Várnai, 2013; Pickard, 2013). If the gene for the LeAGP1 homologue AtAGP19 is deleted from arabidopsis, plants grow poorly with pale green relatively small malformed leaves (Yang *et al.*, 2007), and their cells are abnormal in size, number, shape and packing. Clearly, KRR-AGPs serve important roles during development. Relatively detailed understanding of individual members of the AGP family of 'enigmatic' or 'mystery' proteins (Tan *et al.*, 2010; Lamport and Várnai, 2013) might lead to better agricultural management methods and to generation of improved crop plants.

We hypothesized that the KRR-AGPs achieve their functions by highly specific electromechanical interactions with each other and with other polymers just outside the cell membrane. As a first step toward understanding the biology of KRR-AGPs, we studied fluorescently labelled LeAGP1 both inside transgenic plants and

in a simplified electrostatic environment. Using spinning disc confocal microscopy to prepare 3-D image stacks of turgid cells and plasmolysed cells, we confirmed, using transgenic plants with a modest level of label, that LeAGP1 labelled with enhanced green fluorescent protein (EGFP) is distributed at the interface between the cell wall and cell membrane (data not shown). The labelled AGP formed elaborate structural arrays at this biological surface, with patterns depending on cell type and environmental conditions (an example is shown in the Results). While some behaviours of a kind of secretory AGP, a fraction of gum arabic, have been studied in solution and to some extent on surfaces (Sanchez *et al*., 2008; see also Renard *et al.*, 2012, 2013), it would seem that the diverse complex interfacial arrays observed for KRR-AGPs must derive from interesting electromechanical properties that are not clearly predictable from the general behaviours of gum arabic or even of KRR-AGPs in solution. Therefore, we purified LeAGP1–EGFP from the plants and used atomic force microscopy (AFM) for high-resolution study of some of its basic behaviours on artificial surfaces. Justifying this approach, retrospectively comparing our scanned LeAGP1–EGFP images with a single hard-tapping atomic force micrograph of a gum arabic fraction deposited on mica by Sanchez *et al*. (2008) revealed little resemblance.

Specifically, with AFM we showed that the fluorochrome-tagged LeAGP1 has a strong tendency to form clusters, arcs and rings when spread on mica or on graphite. The rings can constitute single and contiguously grouped 'nanopores'. Depending on substrate and application methods, small flat aggregates, thick sheets and extensive lacy sheets can form. Such AFM studies on simplified substrates have proven to be an effective means of evaluating the behaviour of molecules, including proteoglycans and their interactions in animals (cf. the text by Tsukruk and Singamaneni, 2012). For example, Wilusz and Guilak (2013) used AFM for the first ever analysis of how the pericellular matrix is affected by proteoglycan digestion, and AFM experiments conducted on mica chips form the foundation for the modern understanding of hyaluronan–aggrecan interactions (Seror *et al*., 2011) and interactions between decorin-decorated collagen and apolipoproteins (Witos *et al.*, 2011). The first quantification of cell adhesion by glyconectin proteoglycans in animals was additionally performed using AFM (Popescu *et al.*, 2003). Most pertinent to the present study, Cannon *et al.* (2008) compared the behaviour of extensin on chips and in cells to elucidate its role in cell plate formation in arabidopsis.

Given that the state of the art in the study of conformations adopted by glycoproteins involves study of only small segments through molecular modelling, an important outcome of all of this work is to provide a foundation for initial guesses for molecular models (e.g. Vlachakis *et al.*, 2013) of the arrangements of the KRR-AGP in the periplasmic environment.

Additional information for modelling derives from structures formed when LeAGP1–EGFP is paired on graphite with the β-D-glucosyl Yariv reagent commonly used to assay for AGP function in cells. This pharmacological reagent reacts with AGPs at the cell membrane and causes an inward Ca^{2+} flux that precedes a host of well-known physiological effects (Pickard and Fujiki, 2005). We hypothesized that Yariv might force LeAGP1 into conformations conducive to such influx. Perhaps physiological importance can already be cautiously assigned to the extra-large rings formed when LeAGP1–EGFP is paired on graphite with Yariv. These appear only if the glycoprotein is adhered to the graphite surface before the Yariv reagent is provided. If further experimentation validates suggestions for how the Yariv and KRR-AGP interact, it will also suggest mechanisms by which LeAGP1 itself forms clusters, arcs and 'nanopores' on mica and graphite substrates.

Our broad, interlocked purposes in employing AFM to examine propensities of a KRR-AGP to form surface structures at the molecular level were to enable development of a protocol permitting examination of how other molecules interact with this AGP, to seek hints for better determination of secondary, tertiary and quaternary structure on standard surfaces, to set the stage for further fluorescence microscopy of structure and dynamics in living cells, and to contribute data for modelling the chemical, electrical and mechanical bases for its surface behaviours at all hierarchical levels. We anticipate that AFM data will combine with observation of putatively diverse and complicated dynamics in the periplasm to help interpret the physiological meaning of nanostructures of LeAGP1–EGFP in transgenic plants and its homologues in natural plants.

MATERIALS AND METHODS

Preparation of EGFP-labelled AGP

Seedlings of an *Arabidopsis thaliana* line containing LeAGP1 labelled with EGFP at the N-terminus were described and provided by José Estévez and colleagues (Estévez *et al*., 2006); for preparation of this construct in the lab of Marcia Kieliszewski, see references therein. They were grown to rosette stage at about 22 °C under continuous light. Leaves were harvested into liquid nitrogen and pulverized in a solution of concentrated NaCl containing protease inhibitors from Sigma (P8340). After adding more solution, the slurry was centrifuged at 4 °C for 30 min at 3000 g (29 000 m s^{-2}). Small molecules were removed with PD-10 columns (GE Healthcare Life Sciences) and protein was concentrated using an Amicon Ultra 4 centrifuge filter tube (same source), which also removed molecules below approx. 50 kDa (free EGFP, at about 27 kDa, should be removed by this procedure). The resulting solution was combined with magnetic beads coated with an antibody against GFPs (Abcam ab69315; www.abcam.com). The magnetically constrained beads were washed four times with 0·5 M NaCl, and the EGFP-linked protein was released with 0·2 M glycine-HCl buffer at pH 3·5. Buffer was immediately exchanged with 0·2 M phosphate-citrate buffer at pH 7 by using an Amicon Ultra 1·5 tube. The fluorescence spectrum of the final eluate corresponded to expectation for excitation at 488 nm using a Cary Eclipse Fluorescence Spectrophotometer from Agilent Technologies (Santa Clara, CA, USA). The AGP concentration of the final eluate was 1 μM, but the concentration was known with more precision than the small volume could be measured. For convenience, plating solutions specified for the figures are based on the maximum possible molarity of dilutions. The extract was stored at −80 °C. The AGP was stored as prepared in a solution of high ionic strength, but diluted with water or salt solution for many experiments. Thus, the storage buffer underwent dilution when the protein was diluted. Water used at every stage in preparation and experimentation was purified

with a Thermo Scientific Barnstead Nanopure Ultrapure Water Purification System (resistivity approx. 18·2 MΩ cm).

Solutions of $CaCl_2$ and NaCl were chosen for deposit because recent work of Tan *et al*. (2010) and Lamport and Várnai (2013) demonstrated a conserved, highly repetitive *O*-Hyp-linked arabinogalactan glycomodule with a 'pocket' that binds Ca^{2+} but not Na^{+}; vibration of the module is strongly inhibited by the former as compared with the latter. AGP attached to the chip in the presence of either salt; it was washed with excess water before drying to remove free salt. The two methods of application yielded no substantial differences in assembly on graphite.

Evaluation of LeAGP1–EGFP purity

Based on information from, for example, Estévez *et al.* (2006) about the glycoprotein and on the assumption that it was processed as expected based on the peptide sequence predicted from its gene, it should be released to the apoplast with an EGFP at the N-terminus after removal of the sequence that signals exit from the endoplasmic reticulum (ER). At the C-terminus, it probably had a GPI sited so as to be involved in the export process. However, little is known about the retention of GPI in the periplast and our extensive confocal imaging (not shown) does not suggest an answer; thus it is unclear whether the AGP had GPI linkage either before or after extraction.

The procedure we used for sample preparation seems suitable because a method used by Estévez *et al.* (2006) to prepare LeAGP1–EGFP in bulk from the same transgenics using an antibody column rather than free antibody beads has been reported to yield LeAGP1–EGFP that shows no contamination on western blots if the preparation is maintained below 60 °C. These workers indicated that in their experiments EGFP runs at about 27 kDa and LeAGP1–EGFP from leaves of the transgenics runs as a blur between 130 and 230 kDa, suggesting that our initial filtering procedure should have removed free EGFP or GPI. Nevertheless, the possibility of contaminants that might bind to the beads or the adhered antigen, or formed by antigen breakdown after purification, should be borne in mind. However, our preparation was carried out in the cold, and at no time approached the 60 °C breakdown temperature specified by Estévez *et al*. (2006). Moreover, binding problems are minimized in wash solutions of high ionic strength.

Control AFM scans also address purity

The ultimate criterion of effective purity is whether unsuspected agents possibly carried in test solutions bind to the chips or influence the binding pattern of the LeAGP1–EGFP. As is customary in AFM, chips with control treatments were scanned, addressing sample purity as well as effectiveness of post-deposit washes. The chips appeared clean in the absence of LeAGP1–EGFP application, and no evidence of $CaCl_2$ and NaCl was found. If these salts had adhered to the substrate, crystals should have been seen. We did not obtain sharp images after depositing AGP onto mica chips from low concentrations of the glycoprotein. In accord with general knowledge, films of water on mica are much more tenacious than on graphite even with strenuous drying – perhaps water films and water tension presented a disproportionate problem with small deposits of the glycoprotein. Alternatively, perhaps the interfacial interactions between the mica and glycoprotein cause distortion with disproportionate effects for small deposits. The water controls were informative in showing that scanning of incompletely dehydrated purified water deposits can reveal distinctive patterns in drying films. Such patterns were extensively studied before judging experiments.

Evidence of disparate structures that would indicate impurity was not found in AGP-treated chips. Structures formed by another similarly purified GFP-labelled protein studied in parallel on silica and mica chips did not resemble those formed by the LeAGP1–EGFP (see Supplementary Data Fig. S1).

Confocal microscopy

Seedlings described in the previous section were imaged with a Leica DM16000 microscope fitted with a Yokoyama spinning disc, exciting with a 488 nm laser beam and imaging with a QuantEM EMCCD camera (Photometrics, Tuscon, AZ, USA). The microscope was driven by Slidebook 5·0 software (Intelligent Imaging Innovations, Inc., Denver, CO, USA); images were extracted as tiff files and processed using ImageJ (US National Institutes of Health, http://rsb.info.nih.gov/ij). Abundant detail will accompany publication of microscopic and physiological analyses of the AGP functions.

Yariv reagents

For stock solutions of Yariv reagents (Biosupplies Australia Pty Ltd, Bundoora, Australia), 2 mg of powder were dissolved in 1 mL of 0·15 M NaCl as recommended by the supplier.

AFM and image analysis

Extract and reagents were diluted as specified for each figure, and a few microlitres were deposited on freshly cleaved mica or highly ordered pyrolytic graphite (HOPG) chips (Ted Pella, Inc., Redding, CA, USA). Mica chips were round (1 cm diameter); because they are hydrophilic, applied solutions spread out over their entire surface. Graphite chips were square (approx. 1·2 cm on edge); because graphite is hydrophobic, applied solutions did not spread well. Thus, although deposited quantities are specified as a guide, the amount of protein per chip area is difficult to compare. Solutions were retained on the chip for a few minutes and washed off with an excess (300–500 μL) of purified water (resistivity approx. 18·2 MΩ cm). Drained chips were dried under a stream of N_2. Images were captured in air (35–50 % relative humidity) in light tapping mode using NSC-11 probes (MikroMasch Co., Lady's Island, SC, USA) with nominal resonance frequency 330 kHz, spring constant 48 Nm^{-1} and tip radius approx. 10 nm. Images of Figs 4 and 5 were obtained with a Veeco Dimension 3000 Atomic Force Microscope (Bruker Corp., Billerica, MA, USA), and the others with an Innova Scanning Probe Microscope (Bruker Corp.). For the physics underlying the choice of such scanning methods for soft materials, consult the text by Tsukruk and Singamaneni (2012). Owing to the high solubility of the AGP, it was anticipated that scanning in water would be impracticable. Because any possible success could yield higher resolution, the method was tested anyway. It proved unsatisfactory for our purposes, and the several biopolymer techniques requiring water imaging were thus ruled out.

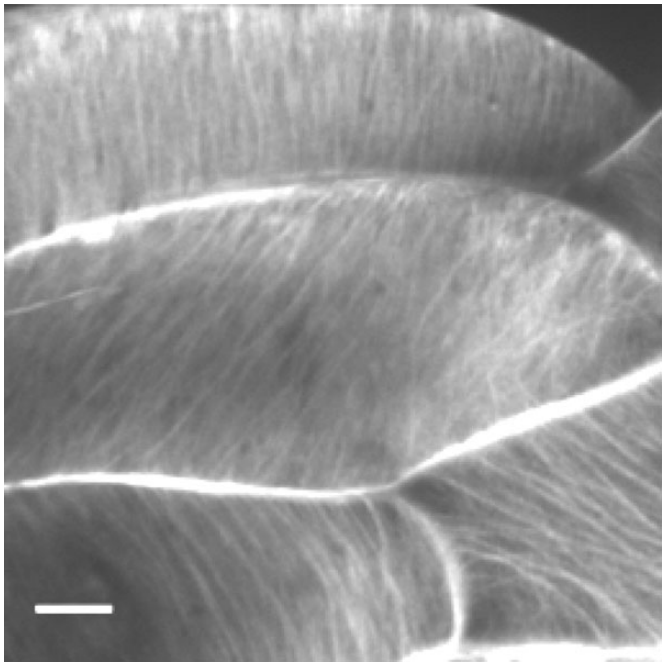

FIG. 1. KRR-AGP is arrayed in distinctive patterns at the exterior side of the cell membrane. The image is a confocal micrograph of cells near the tip of a light-grown hypocotyl of arabidopsis expressing a tomato gene linked to a promoter from *Cauliflower mosaic virus*. The tomato protein is homologous to three arabidopsis AGPs. This figure is introduced to suggest that resolution of form by AFM and confocal microscopy will be complementary for analysis of biological deployment despite large differences in limit of resolution. Perhaps because the expression level in this transgenic line is low, at least after carrying through several generations, no evidence was found for retention of the AGP inside the cytoplasm. Scale bar = 20 μm.

Primary preparation of images was with Nanoscope Analysis 1·40 provided with the instruments (Bruker Corp.) except for one 3-D insert in Fig. 5, for which ImageJ (US National Institutes of Health) was used to indicate sheet depth. It must be kept in mind that the maximal height of structures on images prepared in this way is fairly accurate, though sometimes slightly under-reported for soft structures, but the width is over-reported (e.g. Tsuruk and Singamaneni, 2012).

The major benefit of attaching EGFP to the LeAGP1 was to enable specific comparisons with data from fluorescence microscopy studies represented by Fig. 1. Initially there was concern whether the EGFP, though terminally attached, might appreciably distort protein self-assembly. Images were carefully examined for such effects but none was obvious. The label has a stable 2 × 3 nm β-barrel, detectable with our 10 nm AFM probe (and with larger probes as well). AGP itself forms protuberances of about this size that confound identification. It can be challenging to estimate dimensions of protein features because they often tend to sink in to the surface of the chip, which is not perfectly rigid. In fact, in the reported experiments, the surface roughness of the chip was often disrupted near the edge of protein deposits, indicating atomic interaction between substrate and protein. The effects of the EGFP were judged to be small enough to be of secondary importance for the present study, though of interest for diverse detailed future studies. Each experiment was replicated at least three times.

RESULTS

AGP patterns at the cell surface

Confocal microscopy of transgenic arabidopsis seedling shoots displaying EGFP-labelled LeAGP1 indicated that the glycoprotein is distributed in elaborate structural arrays at the outer surface of cell membranes. Figure 1 exemplifies a type of peripheral pattern common in elongate cells. This image represents a very large set of our spinning disc confocal data obtained with diverse cell types, intended for publication elsewhere. Understanding the formation of structures shown in such studies will require more extensive biophysical, biochemical, genetic and physiological characterization of this glycoprotein and its homologues, both with and without fluorescent label. Because at present our only general method of examining KRR-AGP at high resolution within living cells is by fluorescence microscopy, we elected to initiate AFM studies on LeAGP1–EGFP to best enable early comparisons with our confocal images, and believe that both data sets can suggest ideas about the behaviour of the native molecule at the cell surface. In the long run, AFM is a technique that might well permit ultimate evaluation of possible KRR-AGP interaction with other biopolymers adjacent to the cell membrane.

Clusters, 'nanopores' and 'co-nanopores' of the AGP on graphite

Clusters comprised of small, variable numbers of molecules form when dilute solutions of the protein are plated onto a smooth graphite substrate (left panel, Fig. 2). Rarely, there are smaller mounds that might be comprised of individual molecules. Individually selected clusters from this and a replicate scan (3-D renderings, Fig. 2) commonly show central depressions. Reliable estimation of the lateral slope of the clusters and the slope and depth of these pits is not possible, because a limitation of this technique is that the size of the scanning tip is too large to follow the precise protein contours so closely. Occasionally, small groups of contiguous pitted clusters are seen.

In some scans, clusters are tight, unpitted or feature only a dimple (not shown). Sometimes loose and tight clusters appeared in the same scan. Plating from monovalent and divalent ion solution (NaCl vs. $CaCl_2$) was initially expected to result in small differences in structure because the molecular dynamics of AGP differ when it binds different cations (Lamport and Várnai, 2013). However, no reproducible morphological difference was discerned following plating from relatively high and low concentrations of the two salts. Rather, longer durations of deposition time and of post-wash drying and waiting time before scanning seemed to account for the tighter clusterings observed.

Permitting aliquots of glycoprotein solution deposited on graphite chips to incubate for longer times typically results in formation of more and taller clusters than if left for shorter times. In three of five 15 min incubations of a 10 pM solution in $CaCl_2$, few if any clusters were seen, and in the two others the clusters were very few and small (left side, Fig. 3). However, three treatments identical except that incubations were for 30 min consistently produced the tall clusters seen on the right side of Fig. 3, where results are represented as typical topographic and cross-sectional height scans.

Evidently, the AGP sticks more readily to itself than to the graphite, and seeding of the clusters on the graphite is slow.

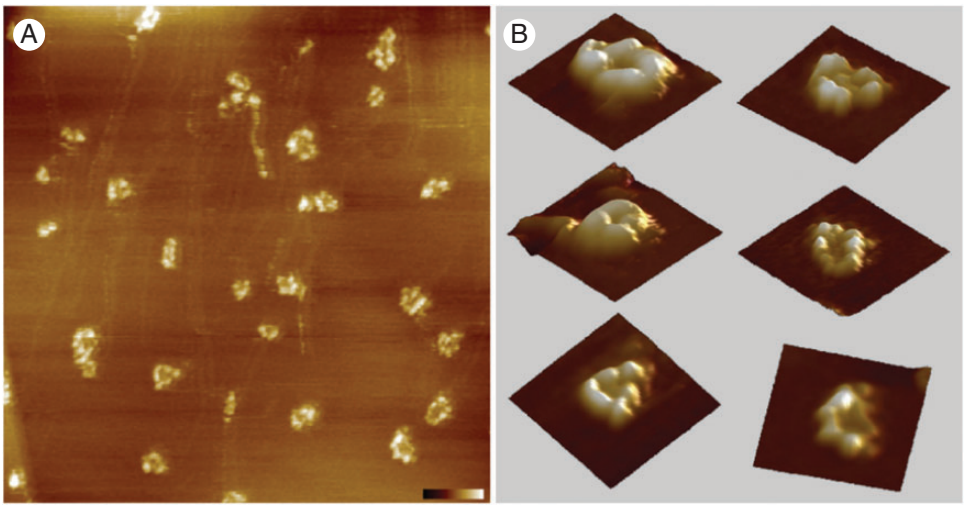

FIG. 2. Clusters form on graphite. (A) This excerpt from a 2 × 2 μm scan of a relatively large area emphasizes that the AGP forms clusters well distributed across a graphite surface. Preparation details: 20 μL of LeAGP1–EGFP drawn from a solution of 10 pM glycoprotein dissolved in 2 M NaCl were deposited on graphite. Adherence of AGP to the graphite surface and development of structure were allowed for 15 min. The graphite chip was then washed with 300 μL of water and dried for 2 min with flowing N_2 before scanning. The colour scale bar indicates a height of 0–6 nm from the lowest part of the graphite surface and is 400 nm long. (B) The 3-D displays of selected clusters from the left image help to visualize the organization of individual clusters. Each display is 200 nm per side.

The important conclusion from such observations is that once deposited the material can serve as a template for further deposition.

Although high-resolution scans of short objects often produce blurry topography, corresponding phase data can be relatively distinct. A 500 × 500 nm scan depicted in phase in Fig. 4 shows clusters of low height: the matched topography view (left) shows little detail, but the phase data (right) make a clear case that the clusters can consist of different molecular arrangements in the centre and outside of the clusters. That is, the topographic blur in Fig. 4 obscures a definitive radial inhomogeneity of structure.

A terminology challenge is presented by the frequent formation of rings and radially inhomogeneous clusters on the impenetrable chip surfaces. Structural geometries grade from outside to the centre and, while some clusters are closed or nearly closed, some are conspicuously open. The word pore comes to mind, but, in the strictest sense, a pore is a hole through which a small object could pass from one side to the other. Here, it would pass from air only to be blocked by graphite. Using a derived definition in accord with modern AFM usage, we name the rings 'nanopores', where quotation marks simply indicate the desirability of further experimental characterization.

Lacy sheets, dense sheets and 'nanopores' of the AGP on mica

Not surprisingly, AGP plated from a $CaCl_2$ or NaCl solution shows a higher affinity for the relatively hydrophilic surface of mica than for graphite. Moreover, when the salt plating solution is washed away following a large deposition, the glycoproteins may bind to each other extensively and may require extra drying. Thus with dense distribution of glycoprotein, scanning immediately after plating shows fairly uniform-looking sheets with small scattered irregularities (not shown). The surface-spread AGP changes form over time. For example, in the 5 × 5 μm scan on the left side of Fig. 5, the surface-spread AGP has resolved into a regular lacy network. It extends uniformly over large areas. The colour scale reveals the topographic depth; however, the inset helps visualize depth because this 3-D representation of a small scanned area includes an approximation of substrate depth. More detail is shown on the right with a 1 × 1 μm scan of the identical chip. Even without the aid of the provided 3-D enlargements, the lace is seen to be comprised of numerous rings, branched rings, joined rings and arcs. The demarcation of the walls of the rings and arcs is very distinct. Central holes are relatively large and reach deep into if not all the way through the sheet. The distinctive rings seen in Fig. 5 are 'nanopores' in the same sense as those observed on graphite. We term the groupings of these rings 'co-nanopores'.

The general pattern seen in Fig. 5 is highly reproducible, although some parameters such as the thickness of wall cross-sections (but not height of walls) may show a considerable range depending on deposit size, incubation time and drying time. When the glycoprotein was applied at a relatively lower concentration, no fine detail could be observed. The protocol of scanning in air used in this study does not offer resolution of molecular detail obtained in the best circumstances with scanning in water, but as noted above the AGP is so soluble that aqueous scanning is impracticable. Moreover, although for some kinds of biopolymers the driest possible specimen is often desired for scanning in air, it is often unclear for the AGP under study whether there should be an absolute preference for one degree of dryness or another. Although dimensions within the lacy sheets appear to shift somewhat in response to a range of desiccating treatments, this may be of secondary importance because the present methodology provides only an introductory view of molecular capabilities.

Comparisons: a summary of AGP formations

Features of the presented images scanned on the relatively hydrophobic graphite surface and scanned on the relatively

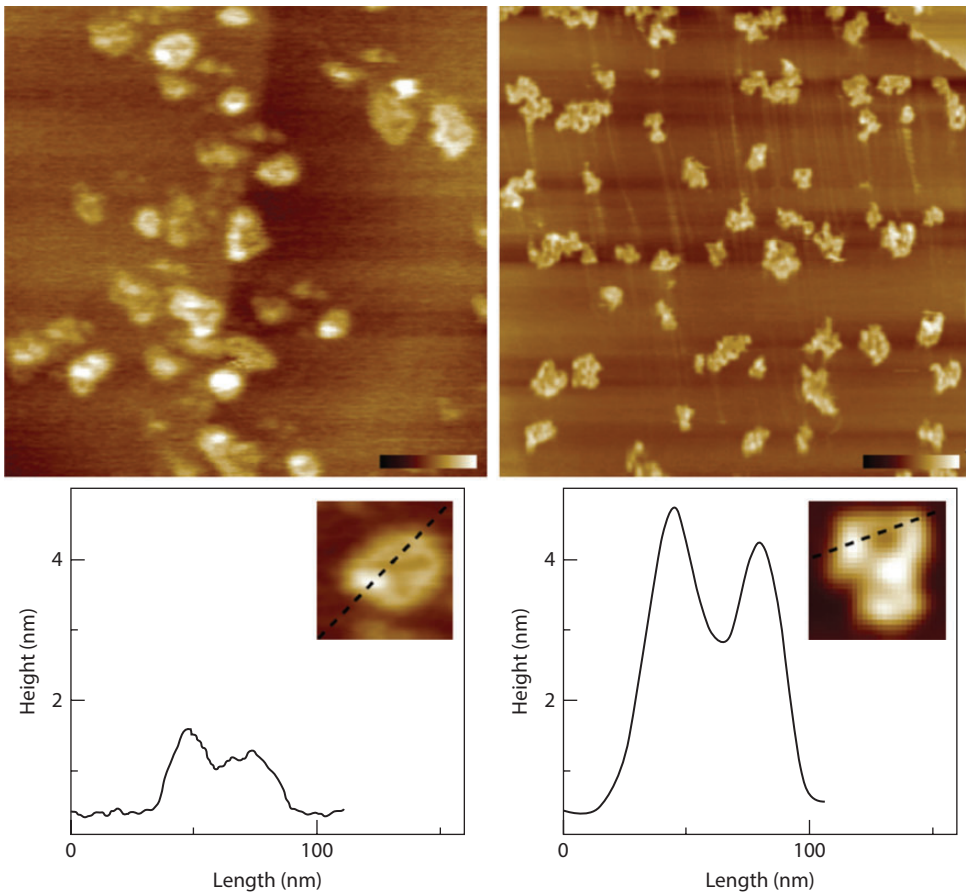

FIG. 3. The height of 'nanopores' on graphite can depend on incubation time. AGP was dissolved in 0·4 M $CaCl_2$ at 10 pM, and 20 μL was deposited on graphite for 15 min (left) or 30 min (right); note differences in scale reported below. 'Nanopores' were typically taller following the 30 min deposition. Below the scans are selected displays of single clusters within the scans, with dotted lines to indicate where the illustrated transections were taken. The left inset display is 70 nm per side, whereas the right is 106 nm. Extremely limited early deposition was observed in three of five replicates of the left scan, and two showed the relatively low structures illustrated. Large deposits of taller structures were seen in all three replicates of the right scan. It is important to appreciate that the scanning procedure tends to yield sharper images for taller topographies. The large streaks on the right scan are probabely a result of protein drag by the AFM scanning tip. The colour bar in the left scan indicates 50 nm length and 0–3 nm height from the graphite surface, and in the right scan 100 nm length and 0–6 nm height. The left scan size is 500 × 500 nm, and the right is 1000 × 1000 nm.

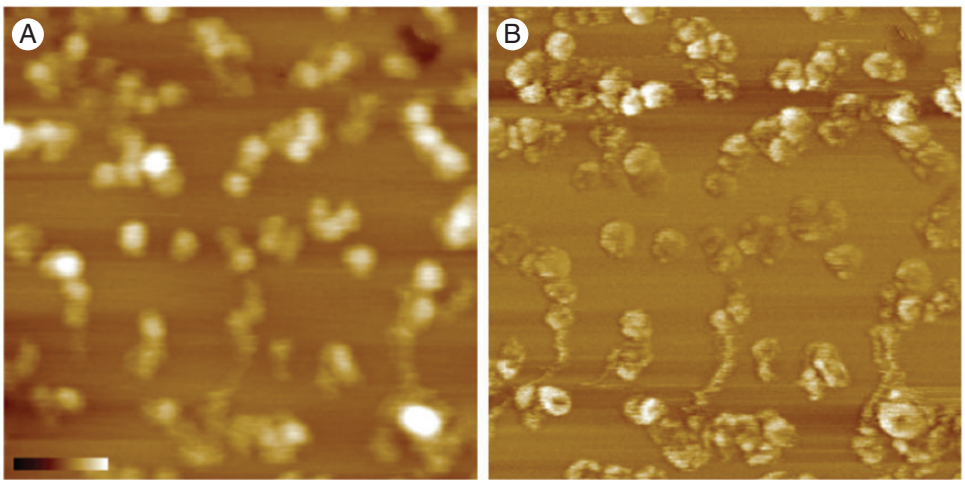

FIG. 4. Phase images confirm radial inhomogeneity of clusters on graphite. The phase image (B) indicates radial inhomogeneity of cluster structure that cannot be resolved in the corresponding topographic image (A) of these relatively short structures. The colour bar indicates a height range of 0–5 nm from the graphite surface in the topographic image on the left and is 100 nm long, whereas for the right image of the identical area, the colour bar represents a range of 0–10° phase shift. The graphite chip was prepared by depositing 2 μL of a 100 pM solution of AGP in 2 M NaCl, waiting 15 min, and then rinsing and drying as in Fig. 1. Streaks may be artefacts due to dragging of protein by the scanning tip. Scan size 500 × 500 nm.

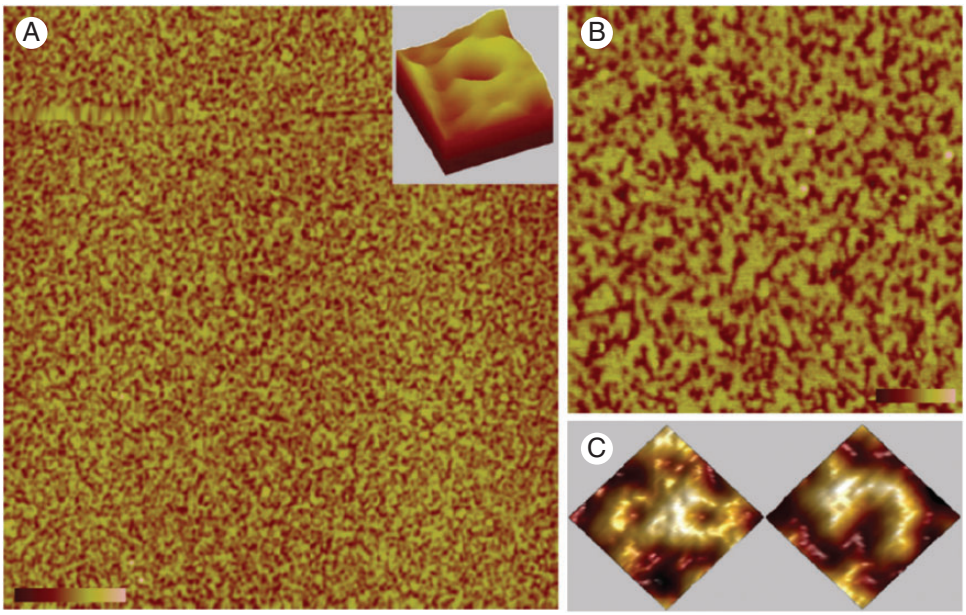

FIG. 5. Lacy sheets on mica are comprised of 'nanoarcs' and 'nanopores'. A deposit of 10 μL of 1 nM AGP in 2 M $CaCl_2$ solution was incubated on mica for 10 min, washed and dried, and maintained in air of 40–50 % relative humidity for 12 h. Initially the sheet was quite smooth in appearance. When re-inspected after 12 h, the molecules formed the pattern seen here. (A) A 5 × 5 μm scan. The colour scale bar represents 2 nm of topological variation and is 300 nm long. The 3-D inset, an enlargement from this scan, is 180 nm per side and indicates that the rim of the pore rests atop a significant layer of AGP. (B) A subsequent 1 × 1 μm scan of a portion of a region within the region plotted in the left panel. The colour scale bar represents 2 nm of topological variation and is 200 nm long. Enlargements (C) are 75 nm on a side.

hydrophilic mica surface are similar enough to permit judgement that the AGP studied can exist as 'nanopores' and 'co-nanopores' when surface-spread from $CaCl_2$ or NaCl solutions, with patterned associations possible between the 'pores' and their arc-like branches.

Strikingly absent from the majority of images were hints of fibrous structure. In a few images, there are some streaks, but they probably represent protein caught and dragged by the scanning tip. Such streaks are a common artefact generated when scanning protein (Ukraintsev *et al*., 2012), and do not exemplify protein self-assembly in the specified environment.

Ring formation with Yariv reagent

The involvement of AGPs in physiological functions is historically shown by application of the pharmacological Yariv phenylglycosides (Ellis *et al*., 2010). These Yariv reagents occur as a set of six stereoisomers. The β-D-glucoside is highly specific for AGP and interferes with diverse cellular functions. Many of these effects have been attributed to rapid Gd^{3+}-inhibited promotion of Ca^{2+} entry into the cytoplasm (Pickard and Fujiki, 2005). The other isomers can be less predictable; for examplem the β-D-mannoside sometimes creates no disturbance and can be used as a control (Pickard and Fujiki, 2005), but sometimes it can be used in place of the always-active glucoside (instructions from the supplier). Salt solution is recommended to solubilize the concentrated reagents, implying a tendency to aggregate in water alone.

Given the cell- or species-dependent stereospecificities of interaction with AGPs and also the interesting symmetry of these compounds (see, for example, the description by the supplier), any structure created when a Yariv reagent reacts with LeAGP1 is instructive. It is particularly interesting if the reactions differ in solution and on surfaces.

Interaction in solution incubated on graphite. When a drop of the AGP solution in 2 M NaCl is incubated with a drop of β-D-glucoside and then deposited on a graphite chip, no structure is observed after sequential washing and drying with N_2. In contrast, if the drop of AGP is deposited on a graphite chip for a few minutes and a drop of the glucoside is then incubated with it, tower-like structures appear immediately after the N_2 drying. As graphed for the scan of Fig. 6, they typically range from 30 to 60 nm in height. Their sturdiness is indicated by the failure of washing to rinse them off; and according to a single experiment they remain unchanged in scans repeated at 2 and 3 d.

Clearly, the AGP and Yariv molecules have the high affinity for each other expected from previous descriptions. However, the geometry of the results could not have been predicted based on past knowledge. When presented to the graphite chip in sequence without drying in between they seem to interact almost as they would in solution, forming some kind of 'pseudocrystalline' array, but rather than plating out a sheet as might have been expected some of the pseudocrystals apparently attract more of the components to themselves and subsequent development of surface energy aids maintenance of towers by resisting downward flow onto the hydrophobic surface of the chip.

Interaction on a graphite surface: large 'nanopores'. In contrast, large flat rings with conspicuous rims appear when a light deposit of AGP dissolved in 2 M NaCl is washed and dried on a graphite surface but then rewetted with β-D-glucosyl Yariv, rewashed and redried (Fig. 7, upper left). The consistently deep

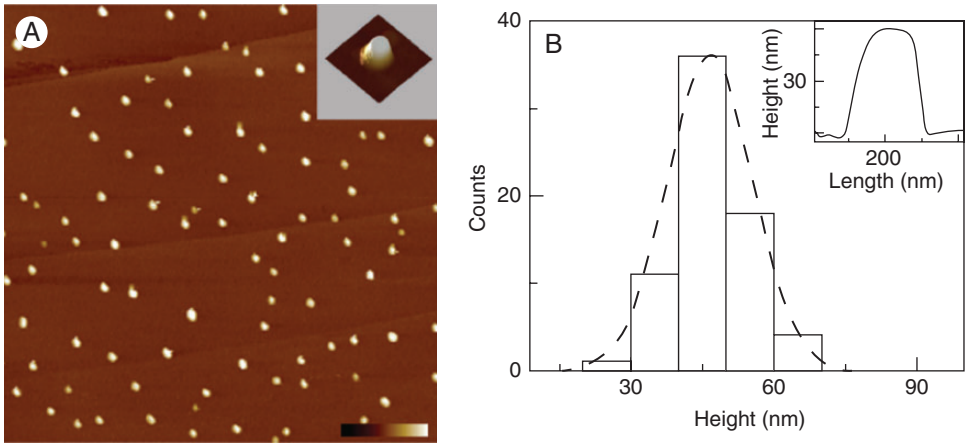

FIG. 6. 'Pseudocrystals' form when LeAGP1 reacts with β-D-glucosyl Yariv reagent in solution. (A) After a 20 μL deposit of 10 pM AGP dissolved in 2 M NaCl on graphite was incubated for 15 min, a 20 μL aliquot of 1 μM glucosyl Yariv reagent was added and another 15 min incubation was allowed. The chip was rinsed with 300 μL of water and dried with N_2 for 2 min. Large discrete 'towers' of 'pseudocrystals' formed. One of the three replicates was rescanned after 2 and 3 d, and the towers did not change form over this period. The colour bar represents 0–100 nm height from the graphite surface and 1 mm length. Scan area 5 × 5 μm. The inserted 3-D figure of a typical tower is 300 nm on each side of its base. (B) Pseudocrystal tower heights were not haphazard. A distribution of tower heights is shown as a bar graph and as a line distribution. A transection of the tower from the inset of the left panel is shown as a graphical insert on the right.

and sharp-edged pits reach the substrate. The ridged edges of the larger 'nanopores' are comprised of a series of incompletely fused peaks, as seen in the 3-D enlargements presented below the upper left scan. The largest peaks on a chip with added glucoside typically rise 3–6 nm above the substrate. Rim diameters measured at the highest points range from 30 to 125 nm, but the median value is about 75 nm (Fig. 7, left).

Yariv alone can form rings. There are numerous small and medium 'nanopores' in the scan of combined glucoside and AGP. A control scan of a chip presented only with the glucoside (Fig. 7, lower left) has similar rings. Thus, the β-D-glucosyl Yariv reagent alone can form 'nanopores' when deposited in such a way that they can lie flat on a surface. In order to better assess any difference between the arrays of 'nanopores' in the upper and lower left panels of Fig. 7, 'nanopore' diameters in the replicate sets of images were measured and binned in the left panel of Fig. 8. Plots of Gaussian curves fitted to the data by a least squares minimization algorithm are also provided.

Composite rings are larger. The distribution of 'simple Yariv' diameters and those from chips to which AGP and β-D-glucosyl Yariv were provided in combination overlap at the lower end of the size scale. However, in a population of 93 composite rings, 22 were larger than any of the 74 controls. The measured diameter exceeds that of controls by up to 29 nm. A Student's *t*-test comparison of the Gaussian fit of the pore size distribution for β-D-glucosyl Yariv reagent alone and that for β-D-glucosyl Yariv reagent with AGP suggested that the two distributions were significantly different ($P < 0{\cdot}01$). Moreover, it is quite possible that the overlapping populations of the left side of Fig. 8 both consist of Yariv reagent alone, and that only the large rings represent interaction of the two molecules.

Mannosyl Yariv with and without AGP. High concentrations of β-D-glucosyl Yariv reagents are consistently toxic to cells expressing perimembrane AGP, so far as is known. The β-D-mannosyl stereoisomer is sometimes toxic (see instructions from the supplier) and sometimes serves as an innocuous control (Gaspar *et al.*, 2004); in our own studies (Pickard and Fujiki, 2005) we have successfully used it as a control against the glucoside. It is thus worthwhile to examine the two stereoisomers plated on graphite with and without LeAGP1. These two experiments are shown on the right side of Fig. 7 and plotted on the right side of Fig. 8.

Images of both mannoside added to surficial AGP and mannoside alone clearly show deep, rimmed pores. However, it is visually conspicuous that not as many very large pores formed as when the glucoside was combined with surficial AGP. Indeed, the right graph of Fig. 8 shows that the median size of both kinds of mannoside peaks is only approx. 40 nm, and pores > 70 nm are rare. The two distributions are tight and closely similar, suggesting absence of interaction of the mannoside Yariv with the LeAGP1: a Student's *t*-test comparing the Gaussian fits of pore size indicated that the distributions were indistinguishable statistically with $P > 0{\cdot}13$.

DISCUSSION

Although an immediate goal of the present study of molecular assembly is to better understand confocal images of an EGFP-labelled AGP with a lysine-rich region in the periplasm of transgenic plant cells, better understanding of how the native glycoproteins perform is of course an ultimate goal. The distinctive structures formed by LeAGP1–EGFP on mica and graphite do not directly clarify the perimembrane physiological organization of either the labelled or the native KRR-AGP, but do suggest styles of behaviour. Based on unpublished confocal images of many cell types, it may be suggested that the KRR-AGPs can form several structural units, depending not only on the cell but also on the position in the cell and on developmental stage and stressful circumstances. Further, the glucosyl Yariv reagent combines with LeAGP1–EFGP on graphite to form a structure that sparks new ideas on how this pharmacological probe permeabilizes cell membranes to Ca^{2+}.

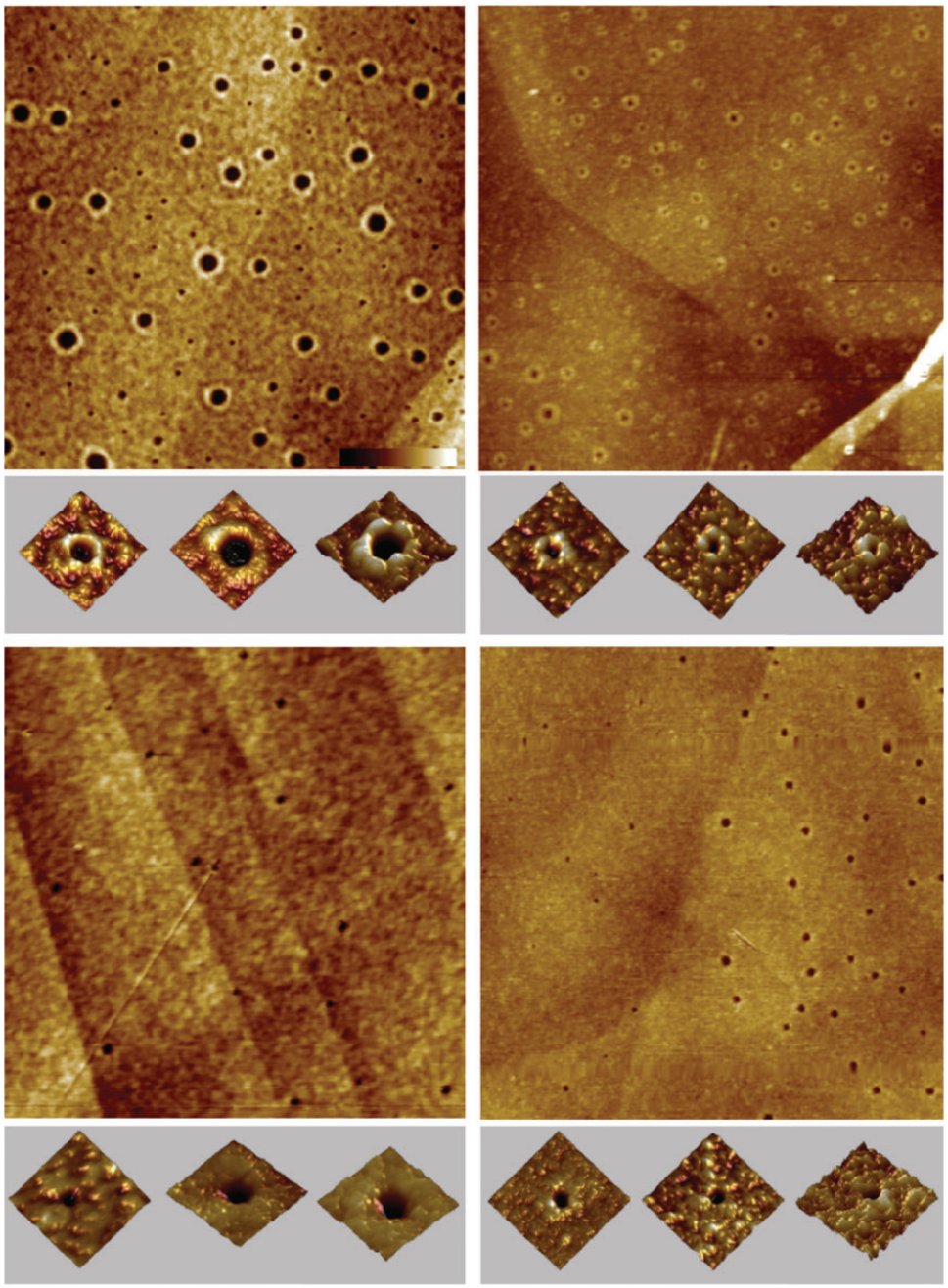

FIG. 7. 'Nanopores' form when the AGP reacts with β-D-glucosyl or β-D-mannosyl Yariv reagent dried on graphite. Upper scans: AGP was plated and incubated as for Figs 2 and 6 and then dried as for Fig. 2. Next, as in Fig. 6, either glucoside (left) or mannoside (right) was added and incubation was permitted for 15 min before rinsing with 300 μL of water and drying. Lower scans: as controls, glucoside and mannoside were added to graphite, without AGP, followed by incubation, rinsing and drying. Combination of the AGP with the glucoside (upper left) yields many relatively large 'nanopores'. Smaller 'nanopores' also occur after combination of AGP and mannoside (upper right). Controls present 'nanopores' in the smaller size range (lower left and lower right). The colour bar indicates a range of 0–6 nm of height from the graphite surface in each control image. The length of the colour bar corresponds to 400 nm; each scan was 2 × 2 μm. Enlarged 3-D images shown beneath each 2 × 2 μm scan are of 'nanopores' formed under each of the four experimental conditions. Each 3-D enlargement is 200 nm per side, and is presented in an orientation chosen to highlight detail. Note: cleavage planes of the graphite are evident, and in the top right and bottom left scans some scratches on the graphite surface are evident.

Before contemplating the biological behaviour of the glycoprotein and contributions from its arabinogalactan modules and lysine-rich sequence, we will evaluate the physically observed LeAGP1 configurations.

Arcs, rings, pores and meshes of the AGP

Assembly on mica. A structural theme emerged during self-assembly of the LeAGP1 into lacy sheets on mica: arcs expressed

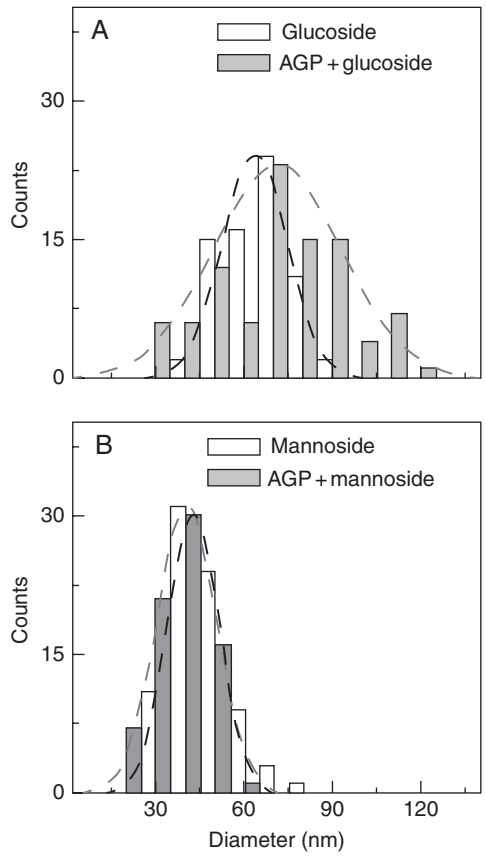

FIG. 8. β-D-Glucosyl but not β-D-mannosyl Yariv reacts with AGP to form enlarged rings. Diameters for the populations of rings in the four scans of Fig. 7 and replicates were measured from the middle of the rim. Although diameter is plotted because it was the measured parameter, the area (which rises as the square of the diameter) may be the more biologically interesting value. Diameters are at 10 nm wide intervals but columns are at half that size to allow the two treatments to be shown together. (A) Glucoside; (B) mannoside. Gaussian trend-lines were fitted to the histograms using a least-squares algorithm.

in both incomplete and complete circles. The arcs typically included several LeAGP1 molecules, associating side by side but with lengths often staggered to fill out circles. Sometimes circles had curved branches, and sometimes multiple circles were united. Central pits often extended to the substrate. The walls of the circles were of variable thickness, suggesting participation of multiple glycoprotein layers, variable coating with water, or both. Indeed, mica is a hydrophilic substrate that seems to encourage the AGP to retain a capillary surface of water, even following relatively extreme measures to dry the deposits.

Assembly on graphite. Structures produced on graphite, although by no means identical to those on mica, shared the arc theme. On this hydrophobic substrate the glycoprotein dried more readily, and the dried surface of clumps and rings looked relatively detailed and irregular. For some rings, the rather lumpy-looking rims tended to surround well-defined pits. In others the lumps tended to press together tightly, suggesting a pore held closed. Although the central pit depth was difficult to evaluate because dimensions were small compared with the radius of curvature of the scanning tip, some pits clearly did not reach the chip surface. Glycoprotein clusters were taller with increasing incubation time on the graphite, suggesting that initially deposited material could serve as a template for further deposition. Reinforcing the concept of a ring motif, the deposits showed radial inhomogeneity regardless of height: both topographic and phase analysis indicated that glycoprotein packed more densely around the outside than on the inside.

Arc structure. Hypothetically, LeAGP1 might form arcs if the bulky glycomodules all point more or less radially outward from the peptide chain. With different chemical affinities on the inside and outside of the curve, the configuration of least energy might present a bend as vibrating glycomodules avoid each other.

However, glycomodules bristling outward from an arc or ring would not fill the circumferential space. Glycomodules from other LeAGP1 molecules might insert, forming a larger arced structure edged with more peptide than glycan. Lateral build-up of this sort, combined with vertical build-up, is consistent with LeAGP1 forms and behaviours on chips, particularly with variability of diameter and height.

Cellular structures of AGP with positively charged sub-domain

Little is published about sub-cellular distributions of LeAGP1. It is considered to form some kind of layer close to the cell membrane, but this is a simplistic generalization based in part on low-resolution cell imaging, in part on extrapolation from assessments of the quantity synthesized by BY-2 cells vs. their estimated cell surface (Lamport *et al.*, 2006), and in part on the fact that it is secreted as a glypiated glycoprotein. Our AFM images and the complexity of the primary LeAGP1 structure combine with our confocal images such as shown in Fig. 1 to suggest strongly that its cellular patternings are polymorphic and that its functions are diverse. Conformations observed on chips can provide only a simplistic foundation for extrapolations about behaviour in the peripheral compartment; nevertheless, they can guide development of testable hypotheses.

Ideas must of course be developed in light of the major differences between environments on the chip and on the cell membrane. Glycoprotein on chips is not constrained except by binding to itself and the substrate, whereas KRR-AGP next to the membrane is probably constrained in at least four ways. First, the perimembrane zone is defined on the one side by lipid head-groups and on the other by layered cellulose. Secondly, KRR-AGP is evidently glypiated when released to the periplasm. Thirdly, the KRR-AGPs under study have by definition an extensive sequence of positively charged amino acid residues, without attached glycomodules: these will obviously have some strong pH-dependent association with the negative surface of the plasma membrane unless they are hidden in structural associations. In other words, they might co-operate with the GPI in anchoring the glycoprotein. Fourthly, LeAGP1 probably interacts with other biopolymers.

With these issues in mind, ideas certainly do arise about the structure and function in the plant; but because they are necessarily speculative and they may be of limited interest except to biologists currently engaging in AGP research – particularly high-resolution optical microscopy – we separate speculations

about cellular distributions consistent with the present AFM data into the Supplementary Data Text.

Glucosyl Yariv reagent

The association of radially inhomogeneous LeAGP1 clusters with β-D-glucosyl Yariv rings to form larger composite rings is of interest both for its own sake and as a prelude to study of LeAGP1 self-assembly into arcs, rings and composites thereof. It was historically known that Yariv reagents can precipitate from solutions of low ionic strength and that glucosyl Yariv reagent combined with AGPs can precipitate even in solutions of high ionic strength. However, detailed information on precipitate structures has been lacking.

Formation of composite rings. Our AFM imaging of both glucosyl and mannosyl Yariv plated on graphite showed that both can form deeply pitted rings, suggesting a pattern of interaction that is not well developed or displayed if it occurs in solution. The absence of distinctive fine-scale pattern on graphite when glucosyl Yariv and the LeAGP1–EGFP were combined before plating is consistent with historical observation. In contrast, extensive bonding was evidenced when the LeAGP1 and glucoside solutions were added to a chip sequentially but without intermediate drying: large, discrete, stable, tower-like structures were formed. Clearly, stronger patterning of interaction could occur on a stable two-dimensional platform. We describe these unusual structures as 'pseudocrystals'. Because it would seem that these comparatively inchoate mounds result from initial modest interaction of the AGP with the surface and subsequent strong interaction between the two molecules in solution, they have little to suggest about behaviour at the surface of the cell membrane.

When a deposit of LeAGP1 was dried before glucoside addition, patterned interaction of the two substances resulted in formation of very large rings – up to 125 nm in diameter. Apparently, only when provided with a flat template consisting of surface-adhered AGP can the glucoside interaction proceed with orderliness sufficient to generate large composite rings. It may be significant that the 'template' consisted of radially inhomogeneous clusters.

Molecular basis of composite rings. Visualization in Fig. 7A of pores formed by interactions between AGP pre-bound to graphite and secondarily added β-D-glucosyl Yariv suggests ways in which the compounds might recognize each other on biological surfaces. Unequivocally, this depends on the stereospecificity of the glucose components of the three-armed Yariv structure and, it may be assumed [see Kitazawa *et al*. (2013)] that it depends on the repetitive large and quintessential *O*-hydroxyproline-linked glycomodule.

We suggest that the relatively small Yariv pores of Fig. 7B and D are helices formed by layering glycosyl units on top of each other in staggered fashion. The hydrogen bond geometry of the sugars should prevent vertical stacking but sequentially encourage offsets that might produce such helices. Helical arrangements in solution have already been proposed (see discussion by Kitazawa *et al*., 2013), but analysis of the helix hypothesis for pore formation on surfaces, using molecular dynamics simulation (see TINKER Molecular Modeling Package on the web), might provide further information.

Such simulation might also help understand the composite rings. Combining structural models of Yariv rings with structural information about glycomodules from Tan *et al*. (2010) and Lamport and Várnai (2013) might indicate whether a glucose arm of Yariv could insert part way between the two glucuronic acids that form the Ca^{2+} binding pocket. A host of alternatives exist, including glucose arms somehow binding between two modules and glucose arms binding directly to short galactan chains more or less as proposed by Kitazawa *et al*. (2013) working primarily with β-D-galactosyl Yariv. Comparison of Figs 7 and 8 indicates that complexities of interaction must exist, and the diversity of interactions of the various Yariv compounds with various AGPs also speaks for complexities, but it is beyond the scope of the present Discussion to imagine them here.

Pharmacological action. The behaviour of AGP in cells treated with Yariv deserves general scrutiny because it bears closely on the pharmacological use of the reagent. Although numerous writers have considered the action of Yariv a mysterious indicator of AGP function, application of β-D-glucosyl Yariv to cultured tobacco cells causes rapid cytosolic Ca^{2+} elevation and Gd^{3+} prevents this. The elevation implicates the appearance of Ca^{2+}-permeable apertures in the cell membrane. Inhibition by Gd^{3+} suggests that they might be mechanosensory channels that open by mechanically pushing against the lipids of the membrane; the very broadly applicable mechanism of inhibition for such channels was shown by Ermakov and colleagues (Ermakov *et al*., 2010) to be interaction of the cation with lipid head-groups of the bilayer near a potentially laterally expanding channel, thus rigidifying the local bilayer and mechanically preventing an increase of the aperture.

The mechanism by which Yariv creates apertures in tobacco cells suggested by Pickard and Fujiki (2005) was that Yariv binding to a cytoskeleton-like AGP force-focusing system opens the previously described (Ding and Pickard, 1993*a*, *b*) mechanosensitive Ca^{2+}-selective cation channels. This remains a strong possibility. (Formally reasonable but unlikely, these channels might themselves be comprised of KRR-AGP in complexes structured to site hydrophobic regions where they could associate with the lipid bilayer.)

Given the new data, an alternative to Yariv action on mechanosensory or other Ca^{2+} channels might be evaluated. Could Yariv form Gd^{3+}-sensitive pores by reacting with widely distributed surface-spread KRR-AGP rings and meshes that are independent of known channels? Could these rest against or at least partially insert in the membrane? Insertion might occur with or without breaking glypiation linkage. Insertion of external protein into the membrane to form pores is of widespread occurrence (Kostka *et al*., 2008; Fantini and Yahi, 2010; Schmidt *et al*., 2012) with bacterial and eukaryote porins. Many porins are permeated by Ca^{2+} (Demuro *et al*., 2011) and some form co-pores (Delcouret, 1997). Based on the study by Ermakov *et al*. (2010), Yariv-provoked ring formation and expansion in the membrane should be inhibited by Gd^{3+}-induced stiffening. Experimental evaluation of the alternatives for creating Ca^{2+}-permeable, Yariv-inducible, perhaps voltage- and mechanosensitive, openings seems possible with microscopy methods (Demuro *et al*., 2011) already used to study porins.

Concluding remarks

The nano-behaviour of LeAGP1–EGFP on artificial substrates should be useful, in combination with other biophysical data, in developing ideas about the assembly of this regulatory glycoprotein at the surface of the cell membrane. Its marked tendency to form arcs and rings suggests that the molecule bends readily, probably finding a low energy state by situating its large carbohydrate moieties on the outside of the bend and its peptide chain on the inside. As more information is gained about the other macromolecules with which the KRR-AGPs probably interact at the cell membrane surface, AFM should be a useful technique for evaluating the geometry of association and complexation.

SUPPLEMENTARY DATA

Supplementary data are available online at www.aob.oxfordjournals.org and consist of the following. Figure S1: an image of another GFP-labelled protein (spectrally confirmed to have YFP rather than EGFP) purified by the same method and observed with the same AFM equipment and technique. Text: a consideration of the possible significance for cellular glycoprotein distribution.

ACKNOWLEDGEMENTS

Support is appreciated from Grant 1102803 to B.G.P. and G.M.G. from the Civil, Mechanical and Manufacturing Innovation Division of the National Science Foundation, from Glenn Allen and Gladys Levis Allen to the Gladys Levis Allen Laboratory of Plant Sensory Physiology, from the Washington University School of Engineering for start-up funds for S.S., from the Major International Joint Research Program of China (11120101002) and National 111 Project of China (B06024) and China Young 1000-Talent Program and Shaanxi 100-Talent Program to F.X., José W. Estévez (University of Buenos Aires, Argentina) and Marcia J. Kieliszewski (Ohio University, USA) shared genes and seeds. Scott L. Crick (Washington University, USA), Joseph M. Jez (Washington University, USA), Jay Ponder (Washington University, USA) and Cynthia Richard-Fogal (recently of Washington University, USA) shared materials and insights. Interaction with David W. Ehrhardt (Carnegie Institute, Plant Biology Department, USA) has been particularly meaningful, and Fig. 1 was captured in his laboratory.

LITERATURE CITED

Cannon MC, Terneus K, Hall Q, *et al*. 2008. Self-assembly of the plant cell wall requires an extensin scaffold. *Proceedings of the National Academy of Sciences of the United States of America* **105**: 2226–2231.

Delcour AH. 1997. Function and modulation of bacterial porins: insights from electrophysiology. *FEMS Microbiology Letters* **151**: 115–123.

Demuro A, Smith M, Parker I. 2011. Single-channel Ca^{2+} imaging implicates Aβ1–42 amyloid pores in Alzheimer's disease pathology. *Journal of Cell Biology* **195**: 515–524.

Ding JP, Pickard BG. 1993*a*. Mechanosensory calcium-selective cation channels in epidermal cells. *The Plant Journal* **3**: 83–110.

Ding JP, Pickard BG. 1993*b*. Modulation of mechanosensitive calcium-selective cation channels by temperature. *The Plant Journal* **3**: 713–720.

Ellis M, Egelund J, Schultz C J, Bacic A. 2010. Arabinogalactan-proteins: key regulators at the cell surface? *Plant Physiology* **153**: 403–419.

Ermakov YA, Kamaraju K, Sengupta K, Sukharev S. 2010. Gadolinium ions block mechanosensitive channels by altering the packing and lateral pressure of anionic lipids. *Biophysical Journal* **98**: 1018–1027.

Estévez JM, Kieliszewski MJ, Khitrov N, Somerville C. 2006. Characterization of synthetic hydroxyproline-rich proteoglycans with arabinogalactan protein and extensin motifs in Arabidopsis. *Plant Physiology* **142**: 458–470.

Fantini J, Yahi N. 2010. Molecular insights into amyloid regulation by membrane cholesterol and sphingolipids: common mechanisms in neurodegenerative diseases. *Expert Reviews in Molecular Medicine* **12**: e27.

Gaspar YM, Nam J, Schultz CJ, *et al*. 2004. Characterization of the Arabidopsis lysine-rich protein that results in a decreased efficiency of Agrobacterium transformation. *Plant Physiology* **135**: 2162–2171.

Kitazawa K, Tryfona T, Yoshimi Y, *et al*. 2008. β-Galactosyl Yariv reagent binds to the β-1,3-galactan of arabinogalactan proteins. *Plant Physiology* **161**: 1117–1126.

Kostka M, Högen T, Danzer KM, *et al*. 2008. Single particle characterization of iron-induced pore-forming alpha-synuclein oligomers. *Journal of Biological Chemistry* **283**: 10992–11003.

Lamport DTA, Várnai P. 2013. Periplasmic arabinogalactan glycoproteins act as a calcium capacitor that regulates plant growth and development. *New Phytologist* **197**: 58–64.

Lamport DTA, Kieliszewski MJ, Showalter AM. 2006. Salt stress upregulates periplasmic arabinogalactan proteins: using salt stress to analyse AGP function. *New Phytologist* **169**: 479–492.

Pickard BG. 2013. Arabinogalactan proteins becoming less mysterious. *New Phytologist* **197**: 3–5.

Pickard BG, Fujiki M. 2005. Ca^{2+} pulsation in BY-2 cells and evidence for control of mechanosensory Ca^{2+} selective channels by the plasmalemmal reticulum. *Functional Plant Biology* **32**: 863–879.

Popescu O, Checiu I, Gherghel P, Simon Z, Misevic GN. 2003. Quantitative and qualitative approach of glycan–glycan interactions in marine sponges. *Biochimie* **85**: 181–188.

Renard D, Garnier C, Lapp A, Schmitt C, Sanchez E. 2012. Structure of arabinogalactan-protein from Acacia gum: from porous ellipsoids to supramolecular architectures. *Carbohydrate Polymers* **90**: 322–332.

Renard D, Garnier C, Lapp A, Schmitt C, Sanchez E. 2013. Corrigendum to 'Structure of arabinogalactan-protein from Acacia gum: from porous ellipsoids to supramolecular architectures'. *Carbohydrate Polymers* **97**: 864–867.

Sanchez E, Schmitt C, Kolodziejczyk E, Lapp A, Gaillard C, Renard D. 2008. The acacia gum arabinogalactan fraction is a thin oblate ellipsoid: a new model based on small-angle neutron scattering and ab initio calculation. *Biophysical Journal* **94**: 629–639.

Schmidt F, Levin J, Kamp F, Kretzschmar H, Giese A, Bötzel K. 2012. Single-channel electrophysiology reveals a distinct and uniform pore complex formed by α-synuclein oligomers in lipid membranes. *PloS One* **7**: e42545.

Seror J, Merkher Y, Kampf N, *et al*. 2011. Articular cartilage proteoglycans as boundary lubricants: structure and frictional interaction of surface-attached hyaluronan and hyaluronan–aggrecan complexes. *Biomacromolecules* **12**: 3432–3443.

Sun W, Zhao ZD, Hare MC, Kieliszewski MJ, Showalter AM. 2004. Tomato LeAGP-1 is a plasma membrane-bound glycosylphosphatidylinositol-anchored arabinogalactan-protein. *Physiologia Plantarum* **120**: 319–327.

Sun W, Xu J, Yang J, Kieliszewski MJ, Showalter AM. 2005. The lysine-rich arabinogalactan-protein subfamily in Arabidopsis: gene expression, glycoprotein purification and biochemical characterization. *Plant and Cell Physiology* **46**: 975–984.

Tan L, Várnai P, Lamport DTA, *et al*. 2010. Plant O-hydroxyproline arabinogalactans are composed of repeating trigalactosyl subunits with short bifurcated side chains. *Journal of Biological Chemistry* **285**: 24575–24583.

Tsukruk VV, Singamaneni S. 2012. *Scanning probe microscopy of soft matter: fundamentals and practices*. Weinheim, Germany, Wiley-VCH.

Ukraintsev E, Kromka A, Kozak H, Remeš Z, Rezek B. 2012. Artifacts in atomic force microscopy of biological samples. In: Frewin C, ed. *Atomic force microscopy investigations into biology – from cell to protein*. InTech. http://www.intechopen.com/books/atomic force-microscopy-investigations-into-biology-from-cell-to-protein.

Vlachakis D, Tsaniras SC, Feidakis C, Kossida S. 2013. Molecular modelling study of the 3D structure of the biglycan core protein, using homology modelling techniques. *Journal of Molecular Biochemistry* **2**: 85–93.

Wilusz RE, Guilak F. 2013. High resistance of the mechanical properties of the chondrocyte pericellular matrix to proteoglycan digestion by chondroitinase, aggrecanase, or hyaluronidase. *Journal of the Mechanical Behavior of Biomedical Materials* **13**: S1751–6161.

Witos J, Saint Guirons J, Meinander K, Dulivo L, Riekkola ML. 2011. Collagen I and III and their decorin modified surfaces studied by atomic force microscopy and the elucidation of their affinity toward positive apolipoprotein B-100 residue by quartz crystal microbalance. *Analyst* **136**: 3777–3782.

Yang J, Sardar HS, McGovern KR, Zhang YZ, Showalter AM. 2007. The lysine-rich arabinogalactan-protein subfamily in *Arabidopsis*: gene expression, glycoprotein purification and biochemical characterization. *Plant Journal* **49**: 629–640.